Is near-spherical shape "the new black" for smoke?

Anna Gialitaki, Alexandra Tsekeri, Vassilis Amiridis, Romain Ceolato, Lucas Paulien, Emmanouil Proestakis, Eleni Marinou, Moritz Haarig, Holger Baars, Dimitris Balis

IS NEAR-SPHERICAL SHAPE "THE NEW BLACK" FOR SMOKE?

Anna Gialitaki [1,2*], Alexandra Tsekeri [1], Vassilis Amiridis [1], Romain Ceolato [3], Lucas Paulien [3] Emmanouil Proestakis [1], Eleni Marinou [1,4], Moritz Haarig [4], Holger Baars [4] and Dimitris Balis [2]

[1] *National Observatory of Athens, IAASARS, Athens, Greece*
[2] *Laboratory of Atmospheric Physics, Physics Department, Aristotle University of Thessaloniki, Greece*
[3] *ONERA, The French Aerospace Lab, Toulouse, France*
[4] *Institute of Atmospheric Physics, German Aerospace Center (DLR), Oberpfaffenhofen, Germany*
[5] *Leibniz Institute for Tropospheric Research (TROPOS), Leipzig, Germany*
**Email: togialitaki@noa.gr*

ABSTRACT

We present smoke lidar measurements from the Canadian fires of 2017. The advected smoke layers over Europe are detected at both tropospheric and stratospheric heights, with the latter presenting non-typical values of the Linear Particle Depolarization Ratio (LPDR) with strong wavelength dependence from the UV to the Near-IR. Specifically, the LPDR values are of the order of 22, 18 and 4% at 355, 532 and 1064 nm respectively. In an attempt to interpret these results, we apply the hypothesis that smoke particles have near-spherical and/or more complicated shapes. Scattering calculations with the T-matrix code revealed that the near-spherical shape is able to reproduce the observed LPDR and LR values of the stratospheric smoke particles at the three measurement wavelengths.

1. INTRODUCTION

Recent studies show that the LPDR of smoke presents large variability ([1] - [5]). Since the LPDR is indicative of particle shape, this variability may be attributed to (a) smoke aerosol mixing with other aerosol types, (b) particles' aging through various atmospheric processes, (c) particle water uptake at different relative humidity conditions. These processes alter the smoke particle shape and composition. Indicatively, the typical LPDR values of aged and fresh tropospheric smoke varies from 2 to 10% at 532 and 355 nm ([1] - [3]), while this value can be larger when smoke is mixed with high depolarizing aerosol types (i.e. dust) ([4] - [5]). Lately, observational evidence of LPDR values that exceed the typical range has been reported. Burton et al. 2015 [6], showed air-borne HSRL measurements of smoke at 8 km altitude, originating from Canadian fires, revealing LPDR values of the order of 20, 9 and 1.8 % at 355, 532 and 1064 nm, respectively. These are also the first reported measurements of smoke LPDR spectral dependence. Other studies validate these high LPDR values for stratospheric smoke particles at 532 nm ([7] - [9]).

In the spotlight of the large-scale Canadian fires of 2017, this unique feature of high values of LPDR with unexpected high spectral dependence for smoke particles raises once again an interesting discussion. Here, we aim to seek for an explanation on the variation of LPDR and LR from UV to Near-IR under the hypothesis that the smoke particles have a near-spherical shape.

Our hypothesis and presented results are a continuation effort on previous work reported in the literature. Specifically, in Mishchenko et al. 2016 [10], the lidar measurements presented in [6] were reproduced considering near-spherical shapes for the smoke particles with an axial ratio 0.9 to 1.2. In Bi et al. 2018 [11], it was showed that the LPDR of near-spherical particles with refractive index of 1.3-1.7 + i0.001- i0.01, can take values up to 100%, depending also on the particle size parameter. However, the results of these studies are limited in terms of reproducing only the LPDR wavelength dependence. Here we make a step further, reproducing also the wavelength dependence of the LR considering near-spherical particles. Our methodology is summarized in Section 2, our results in Section 3 and we conclude in Section 4.

2. METHODOLOGY

2.1 The BERTHA lidar system

The lidar measurements presented in this study were conducted at the Leibniz Institute of Tropospheric Research (TROPOS), with BERTHA (Backscatter Extinction lidar-Ratio Temperature Humidity profiling Apparatus) multi-wavelength lidar system [12]. BERTHA optical setup is based on two Nd:YAG lasers emitting linearly-polarized light at three wavelengths (355, 532 and 1064 nm) with a repetition rate of 30 Hz, and a 53 cm Cassegrain telescope collecting the backscattered light. The measurements have a 7.5 m and 5-30 sec vertical and temporal resolution, respectively. The receiver unit employs 13 photon-counting channels in total. The capability of BERTHA to provide independent measurements of the particle extinction coefficient and LPDR at three wavelengths constitutes this lidar system unique within the EARLINET network [13]. The BERTHA measurements used herein are not simultaneous for the particle extinction coefficient and LPDR at 1064 nm, since the 1064 cross-polarized channel had to be exchanged with the 1058 nm rotational Raman channel in order to measure the particle extinction at 1064 nm. The overall duration of this procedure was 20-30 minutes [14]. This shortcoming is not expected to affect the study, since the scene analysed is very stable in terms of aerosol layering, especially in the stratosphere (Figure 1).

2.2 Scattering calculations

In order to reproduce the unique values and spectral dependence of the LPDR and LR of the stratospheric smoke from the Canadian fires, we used light scattering calculations generated with the T-matrix code [15, 16]. The T-matrix code is based on the exact numerical solution of Maxwell's equations. For the calculations we considered a wide range of refractive indices and effective radii typical for aged smoke, employing near-spherical particles but also soot fractal aggregates.

3. RESULTS

Figure 1 presents the observations from Leipzig, on August 22nd 2017, with the 3+3+3 polarization/Raman lidar BERTHA. As it can be seen from the Range Corrected Signal (RCS) at 1064 nm, the stratospheric smoke layer lies between 15 and 16 km, while there is also a smoke layer in the troposphere at 5-6 km. For deriving the smoke optical properties, lidar signals were averaged over a time window of 2.5 hours (20:45 – 23:15 UTC) to achieve satisfying signal to noise ratio (SNR), even at high altitudes. For deriving the LPDR at 1064 nm a time window of 40 min was used (23:50 – 00:30 UTC).

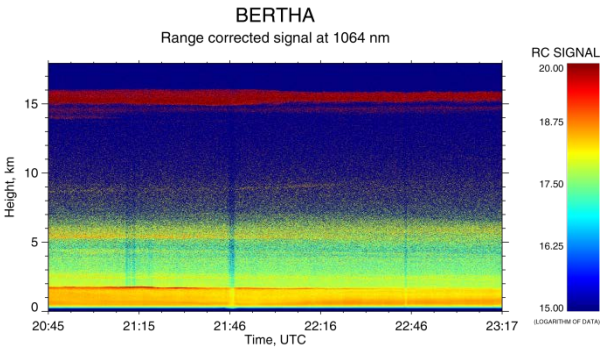

Fig.1. BERTHA RCS at 1064 nm, showing the smoke layers advected from Canada over Leipzig, in the troposphere (5 – 6 km) and in the stratosphere (15 – 16 km).

Figure 2 shows the mean LPDR and LR of the stratospheric smoke layers. The LR values are found to be typical for aged smoke particles (40 ± 16) sr at 355 nm, (66 ± 12) sr at 532 nm, which are consistent with what is reported in the literature (i.e. [1] – [5], [17] - [18]), and (92 ± 27) sr at 1064 nm. No significant difference has been detected for the LR values between the tropospheric and stratospheric layers (for the first one LR is not presented here), while this does not hold true for the LPDR values. In the case of stratospheric smoke the LPDR values are 22.5, 18.5 and 4% at 355, 532 and 1064 nm, respectively, while in the troposphere they are no higher than 3% at all wavelenghts.

Building on the previous studies of [10] and [11] we used near-spherical smoke particles to reproduce the measured LPDR and LR at 355, 532 and 1064 nm in the stratosphere. T-matrix simulations were conducted for a range of refractive index values: m = 1.4 – 1.65 (with step of 0.05) + i0.005 – 0.04 (with step of 0.005), effective radius: r_{eff} = 0.25 – 0.45 μm (with step of 0.05) and axial ratio: a/b = 0.7 – 1.2 (with step of 0.05). Figure 3 presents the best fit of the

measured LPDR and LR at 355, 532 and 1064 nm, calculated for near-spherical smoke particles with axial ratio of 1.1, m = 1.42 + i0.02 and r_{eff} = 0.55 μm (Figure 4). Table 1 summarizes the results of our simulations for near-spherical particles, in comparison with the Leipzig observations.

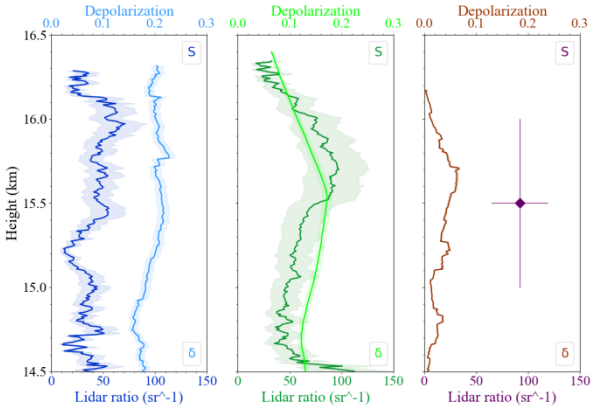

Fig.2) Vertical profiles of LR and LPDR (355, 532 and 1064 nm) of stratospheric Canadian smoke. All profiles correspond to the time window 22/8 20:45 – 23:15 UTC, except of the LPDR at 1064 nm which corresponds to the time window 23:50 – 00:30 UTC.

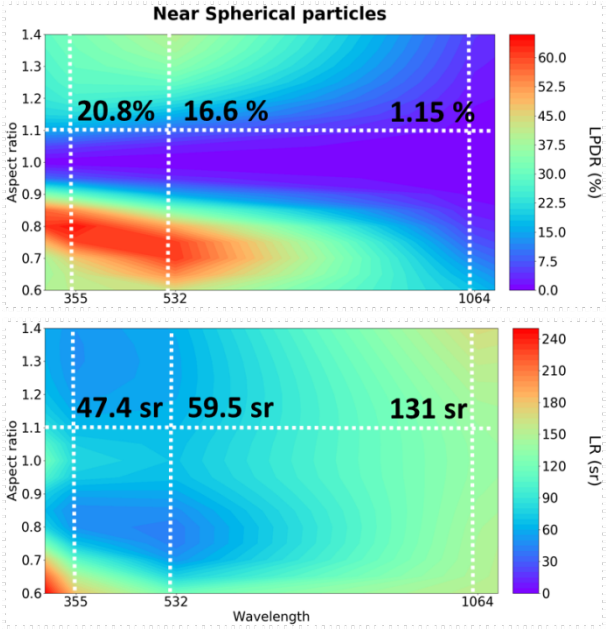

Fig. 3) LPDR and **b)** LR, calculated with the T-matrix code for near-spherical smoke particles with r_{eff} = 0.55 μm, v_{eff} = 0.02 and m = 1.42 + i0.02. The measured LPDR and LR at 355, 532 and 1064 nm are reproduced for near-spherical smoke particles with aspect ratio = 1.11 (white dash lines).

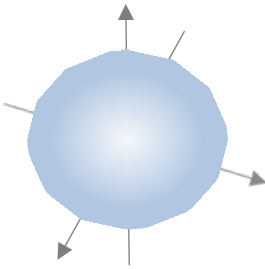

Fig. 4) Near spherical particle (a/b = 1.11, r_{eff} = 55 μm) used to reproduce the LPDR and LR values.

The T-matrix-calculated LPDR values were found to be 20.8, 16.6 and 1.15 % at 355, 532 and 1064 nm respectively, while the LR values were 47.4, 59.5 and 131 sr at 355, 532 and 1064 nm. A slight deviation from the measured mean values is found at all wavelengths, with maximum for the LR value at 1064 nm. However, it has to be noted here that the retrieval of the LR at 1064 nm from BERTHA measurements had an uncertainty of the order of 50% [14]. This uncertainty comes from the fact that the 1058 nm signal Raman returns were too weak from the stratospheric height of 15-16 km to derive the particle extinction coefficient at 1064 nm. To compensate this, a least-squares linear regression method has applied with a vertical smoothing window of 2500 m in the stratosphere. This treatment yielded to LR values in the range of 65 to 119 sr at 1064 nm. The methodology is described in detail in [14].

Table 1. Leipzig measurements vs T-matrix simulations for near spherical particles for a/b = 1.1, m = 1.42 + i0.02 and r_{eff} = 0.55μm.

	355	532	1064
		LPDR	
Obs.	22.4 ± 1.5	18.4 ± 0.6	4.3 ± 0.7
Sim.	20.8	16.6	1.15
		LR	
Obs.	40 ± 16	66 ± 12	92 ± 27
Sim.	47.4	59.5	131

In an attempt to more-precisely reproduce the observed measurements, we also performed scattering calculations with the Superposition T-Matrix Method (STMM) [19] for highly irregular smoke particles with a simple chain-like fractal morphology (Figure 5).

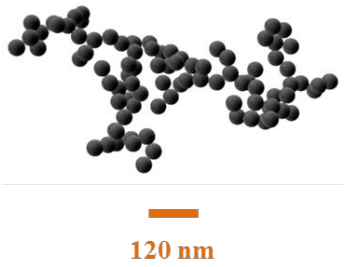

Fig. 5) Chain-like model morphology of soot fractal aggregate used in STMM simulations.

Specifically, we considered a soot fractal aggregate with a fractal geometry provided by a diffusion-limited cluster-aggregation (DLCA) model [20]. Here, the complex refractive index is 1.42 + i0.02 and the fractal morphology of the particle is characterized by the fractal pre-factor $k_f = 1.3$, the fractal dimension $D_f = 1.8$, the number of monomers $N = 90$, and the volume-equivalent radius $R_V = 0.55\ \mu m$. The calculated LPDR of the fractal soot aggregate at 355, 532 and 1064 nm are presented in Table 2. The use of simple chain-like fractal geometry provides significantly large LPDR andreproduces the LPDR values of fresh smoke (~10% at 532 nm[1] - [3]). In order to reproduce higher depolarization by aged smoke, more complex fractal geometry should be investigated.

Table 2. Leipzig measurements vs superposition T – matrix simulations for a fractal aggregate with m = 1.42 + i0.02, $D_f = 1.8$, $k_f = 1.3$, $R_V = 0.55\ \mu m$.

	355	532	1064
		LPDR (%)	
Obs.	22.4 ± 1.5	18.4 ± 0.6	4.3 ± 0.7
Sim.	13	10	3

D_f = 1.8, k_f = 1.3, R_v = 0.55 μm

4. CONCLUSIONS

Near-spherical assumption explains at a large extent the exceptional LPDR values observed at stratospheric smoke layers over Leipzig, Germany, originated by Canadian wildfires. This hypothesis also reproduce the high LPDR spectral dependence found, when the aspect ratio is very close to unity for typical refractive index, and size of smoke particles. The assumption of soot particles with more complicated morphology used here, is not reproducing the observations. The next step is to extend our analysis of monodispersed near-spherical smoke particles, to the retrieval of the microphysical properties of pollydispersed near-spherical smoke particles in the stratosphere.

ACKNOWLEDGEMENTS

We acknowledge support of this work by the project "PANhellenic infrastructure for Atmospheric Composition and climatE change" PANACEA (MIS 5021516), the Stavros Niarchos Foundation and the European Research Council under the European Community's Horizon 2020 research and innovation framework program / ERC Grant Agreement 725698 (D-TECT).

REFERENCES

[1] D. Müller et al. J. Geophys. Res., 110, D17201, 5 (2005)
[2] D. Nicolae et al. J. Geophys. Res. Atmos., 118, 2956–2965 (2013)
[3] E. Giannakaki et al. Atmos. Chem. Phys., 15, 5429–5442 (2015)
[4] Tesche et al. J. Geophys. Res. 114, D13202 (2009)
[5] I. Veselovskii et al. Atmos. Meas. Tech., 11, 949-969 (2018)
[6] S. P. Burton et al. Atmos. Chem. Phys., 15, 13453 – 3473 (2015)
[7] M. Fromm et al. J. Geophys. Res. Atmos, 113 (2008)
[8] N. Sugimoto et al. SOLA, 6, 93–96 (2010)
[9] F. Dahlkötter et al. Atmos. Chem. Phys., 14, 6111–6137 (2014)
[10] M. Mishchenko et al. Applied optics, 55, 9968–9973 (2016)
[11] L. Bi et al. Opt. Express, 26 (2018)
[12] M. Haarig et al. Atmos. Chem. Phys., 17, 10767–10794 (2017)
[13] G. Pappalardo et al. Atmos. Meas. Tech., 7, 2389–2409 (2014)
[14] M. Haarig et al. Atmos. Chem. Phys., 18, 11847-11861 (2018)

[15] P. C. Waterman, Phys. Rev. D, 3, 825 – 839 (1971)
[16] M. Mishchenko et al. J. Quant. Spectrosc. Radiat. Transfer, 60, pp. 309—324 (1998)
[17] T. Murayama et al. Geophys. Res. Lett., 31, L23103 (2004)
[18] M. Fiebig et al. J. Geophys. Res. Atmos., 107 (2002)
[19] D. W. Mackowski, J. Quant. Spectrosc. Radiat. Transfer 133, 264–270 (2014)
[20] S. Jungblut et al. J. Phys. Chem. C, 123 (1), 950–954 (2019)